MODERATE RESOLUTION PROFILE STRUCTURE OF THE SARCOPLASMIC RETICULUM MEMBRANE UNDER LOW TEMPERATURE CONDITIONS FOR THE TRANSIENT TRAPPING OF E_1~P

DONATELLA PASCOLINI AND J. KENT BLASIE
Department of Chemistry, University of Pennsylvania, Philadelphia, Pennsylvania 19104

ABSTRACT The calcium uptake reaction kinetics of isolated sarcoplasmic reticulum (SR) vesicles have previously been shown to be at least biphasic over a range of temperatures (26 to −10°C) with a fast phase identified with the formation of E_1~P and calcium occlusion and a slow phase with Ca^{2+} translocation across the membrane and turnover of the Ca^{2+}ATPase ensemble. At "low" temperatures, namely 0°C or lower, E_1~P formation is slowed and E_1~P is transiently trapped for at least several seconds, as indicated by the absence of the slow phase for 6 s or more. We now report that a reversible, temperature-induced structural transition occurs at about 2–3°C for the isolated SR membrane. We have investigated the nature of this structural transition utilizing meridional and equatorial x-ray diffraction studies of the oriented SR membrane multilayers in the range of temperatures between 7.5 and −2°C. The phased meridional (lamellar) diffraction has provided the profile structure for the SR membrane at the highest vs. lowest temperature at the same moderate resolution of 16–17 Å while the equatorial diffraction has provided information on the average lipid chain packing in the SR membrane plane in the two cases. To identify the contribution of each membrane component in producing the differences between the profile structures at 7.5 and −2°C, step-function models have been fitted to the moderate resolution electron density profiles. Lipid lateral phase separation may be responsible for inducing the structural change in the Ca^{2+}ATPase, thereby resulting in the slowing of E_1~P formation and the transient trapping of E_1~P at the "lower" temperatures.

INTRODUCTION

The sarcoplasmic reticulum (SR) membrane regulates the levels of intracellular Ca^{2+} during muscle contraction and relaxation: this process requires an ATP-driven active transport of calcium from the cytoplasm into the sarcotubular system across the SR membrane against a calcium concentration gradient and it is mediated by a membrane-bound Ca^{2+}ATPase protein (1–3). According to a minimal scheme proposed by DeMeis and Vianna (4) and widely used in literature, the transport process consists of a closed cycle of partial reactions involving a number of distinct chemical intermediates for the Ca^{2+}ATPase protein. In extensive x-ray and neutron diffraction studies (5–7), hydrated oriented multilayers of SR membranes (highly purified to contain nearly exclusively phospholipids and the Ca^{2+}ATPase protein) were utilized to determine the separate profile structures of the lipid bilayer and the Ca^{2+}ATPase molecule within the membrane profile at ~10 Å resolution. These structural studies have shown that the Ca^{2+}ATPase molecule spans the lipid bilayer with a substantial portion of its mass occurring outside the lipid polar headgroups on the extravesicular side of the membrane profile and an asymmetry of the lipid bilayer with regard to the number of lipid molecules in the inner vs. outer monolayer and with regard to the fatty-acyl chain extension in the two monolayers (for details see reference 7).

The SR membranes in the oriented multilayers are fully capable of ATP-induced calcium uptake, like the homologous vesicular dispersions (5–8). By experiments which utilized double-beam spectrophotometric techniques and the metallochromic indicator arsenazo III to detect the Ca^{2+} transport process and the flash photolysis of caged ATP (9) to synchronously initiate the calcium transport cycle for the ensemble of the Ca^{2+}ATPase molecules in the multilayer, the calcium uptake kinetics have been shown to be at least biphasic at all the temperatures in the range between 26 and −10°C (8, 10, and Fig. 2 of reference 11). A fast phase is identified with the formation of the first phosphorylated intermediate of the Ca^{2+}ATPase, E_1~P, and calcium occlusion, a slow phase is identified with the translocation of Ca^{2+} across the membrane profile and turnover of the enzyme ensemble. Both phases of the Ca^{2+} uptake kinetics are progressively slower with decreasing temperature. At temperatures of 0°C or lower the slow phase does not appear until 6 s or more into the plateau of the fast phase, indicating the transient trapping of the first phosphorylated intermediate (12–16). The effect of the

transient trapping phenomenon is only of increasing the lifetime of the E_1~P intermediate, without altering the turnover capability of the enzyme.

We now report that the SR membrane structure undergoes a reversible, temperature-induced structural transition at abou 2–3°C. This transition was detected by the evolution of the meridional and equatorial x-ray diffraction from oriented SR membrane multilayers over the temperature range 8 to −2°C and produces significant changes in the relative intensities of the meridional diffraction orders arising from the SR membrane profile structure and in the equatorial diffraction arising from the average lipid chain packing in the SR membrane plane. The electron density profiles for the SR membrane below and above the temperature of the transition have been calculated at 16–17 Å resolution and they are quantitatively compared by means of step-function models. Because the transient trapping of the first phosphorylated intermediate of the Ca^{2+}ATPase enzyme is mediated solely by the lower temperature under these experimental conditions, it is of particular interest to compare the structure of the SR membrane above and below this structural transition to identify the structural changes in the lipid and protein components and thereby the structural requirements at molecular level responsible for slowing the formation and the transient trapping of E_1~P.

This work has been previously reported in abstract form (17).

METHODS

Oriented multilayers of isolated, highly purified SR membranes (Ca^{2+}ATPase content >90% of the protein with ~10^5 mol wt) were prepared as previously described (5–7, 11) by partial dehydration under sealed conditions at a relative humidity of 88% at the chosen temperature. The cylindrically curved multilayers were mounted in sealed canisters to be positioned in a temperature-regulated (water-cooled) x-ray specimen chamber, the relative humidity within the canister being controlled via a saturated salt solution. The canisters possess x-ray entrance and exit windows of thin (6 μm) Mylar, which are matched by appropriate ports in the specimen chamber.

For the meridional diffraction, the x-ray beam (Ni-filtered CuKα x-rays from an Elliott GX-6 rotating anode generator, Marconi Avionics Ltd., Borhamwood, England) was line-focused at the detector via single mirror Franks' optics (18) and was directed for tangential (grazing) incidence to the multilayer surface with the line-focus parallel to the multilayer surface. The diffraction was recorded in consecutive exposures of 5 min on a linear position-sensitive detector placed at 640–650 mm from the center of the multilayer. Exposures that exhibited no evolution of the sample were summed together to cumulative exposures ranging from 4 to 18 h. The one-dimensional record of x-ray counts vs. the corresponding 1,024 digital locations on the linear position-sensitive detector thus obtained represents the one-dimensional meridional (lamellar) intensity function $I(z^*)$ vs. the reciprocal space coordinate z^* ($|z^*| = 2\sin\theta/\lambda$) inclusive of the background scattering function. The background scattering functions were determined for each pattern and removed; they consisted of a piecewise continuous exponential function fitted to the four regions of constant phase of the intensity function. Approximate multilayer lattice periodicities d and reciprocal space origins $z^* = 0$ were determined for the background subtracted intensity functions from the slope and intercept of the straight line fit to the diffraction order peak center positions (at $z^* \sim \ell/d$ for ℓ integer) vs. z^*. A further correction proportional to z^* squared was applied to the intensity data allowing for the cylindrical curvature and mosaic spread (lattice misorientation) of the multilayers which were then subjected to Fourier analysis to obtain the correct multilayer unit cell electron density profiles.

The equatorial diffraction was observed utilizing Ni-filtered CuKα x-rays produced by an Elliott GX-13 generator (Marconi Avionics Ltd.) with the beam at normal incidence to the multilayer surface, recorded on a two-dimensional x-ray detector (model X-100, Nicolet Instrument Corp., Madison, WI) and stored on computer disk (model 9000, Cadmus Computer Systems Inc., Lowell, MA) as two-dimensional arrays of 512 × 512 elements. The beam was line-focused via single mirror Franks' optics (18) utilizing a 200-mm Ni-coated mirror and the length of the line reduced by slits to 1 mm. In these equatorial diffraction experiments, the beam is thereby incident normal to the planes of the SR membranes in the oriented multilayer and the diffraction arises from the membrane electron density contrast projected onto the membrane plane. Using cylindrical coordinates r, ϕ, z for the SR membranes in the multilayer with z normal to the membrane plane, the equatorial diffraction intensity is expressed as $I(r^*, \phi^*, z^* = 0)$ where r^*, ϕ^*, z^* are the reciprocal coordinates. Angular integration over 2π of this intensity function yields a one-dimensional intensity function $I(r^*)$ defined as

$$I(r^*) = \int_0^{2\pi} I(r^*, \phi^*, z^* = 0)\, d\phi.$$

For each diffraction pattern a corresponding background pattern of identical exposure time was collected containing the scattering from the x-ray optics, slits, windows, and from the multilayer substrate (Al foil). Equatorial diffraction under identical experimental conditions was also similarly collected from oriented multilayers of dipalmitoyl phosphatidylcholine, DPL (Sigma Chemical Co., St. Louis, MO) at room temperature, i.e., below the phase transition temperature for chain melting. The typical sharp reflection at 1/4.2 $Å^{-1}$ was used to calibrate the r^* axis and determine the positions of the equatorial diffraction maxima from the oriented SR multilayers.

All data reduction and analysis for the lamellar and the equatorial diffraction experiments were performed using a VAX 11/750 computer system (Digital Equipment Corporation, Marlboro, MA).

RESULTS

Temperature Dependence of Meridional Diffraction

To determine the profile structure of the sarcoplasmic reticulum membrane at −2°C and to compare it with the profile structure at 7.5°C, three different experimental approaches were used. The first consisted of recording the meridional (lamellar) x-ray diffraction from oriented multilayers fully equilibrated at −2°C (or 7.5°C) after their partial dehydration at that temperature, −2°C (or 7.5°C) respectively, for 16–18 h. In the second approach the oriented multilayers were partially dehydrated at 7.5°C and subjected to a slow slewing of the temperature from 7.5°C to −2°C over a 2–4–h period; the multilayers were then either subjected to a fast reversal (~5 min) of the temperature at 7.5°C or maintained at −2°C for several hours. The meridional diffraction was recorded throughout this slewing of the temperature with consecutive x-ray exposures of 5 min each referenced to the mean temperature over the 5 min interval. In the last approach, a set of multilayers was partially dehydrated for 16–18 h, each multilayer in the set at a different temperature in the range between 7.5 and −2°C at intervals of about half a degree;

the meridional diffraction was recorded for each multilayer in the set fully equilibrated at the temperature of partial dehydration. Because the meridional diffraction is markedly different for multilayers partially dehydrated at the higher temperatures, 7.5 to 2–3°C, vs. the lower temperatures, 2–3 to −2°C, the last two experimental approaches were devised to obtain information on the temperature dependence of the process.

The meridional (lamellar) x-ray diffraction intensity functions $I(z^*)$ typical for oriented multilayers of SR membranes prepared according to the experiments outlined above, recorded by a x-ray linear position-sensitive detector, are shown in Fig. 1. Fig. 1 *A* is the meridional intensity function (4 h cumulative exposure) for a multilayer fully equilibrated at 7.5°C. Fig. 1 *B* is the intensity function (4 h cumulative exposure) for the same multilayer at the final point of the slow slewing of the temperature described above and thereby only partially equilibrated at −2°C. Fig. 1 *C* is the intensity function (18 h cumulative exposure) for a multilayer fully equilibrated at −2°C. The meridional intensity functions contain diffraction maxima corresponding to the anticipated positions of the first $\ell = 1$–11 orders of lamellar diffraction at $z^* \simeq \ell/d$ for disordered multilayer lattices with periodicities of 207–211 Å. The relative intensities of all the orders vary with the change in temperature from 7.5 to −2°C, most markedly the relative intensities of $\ell = 3$ and $\ell = 4$, while the lattice periodicity remains constant. The changes are more pronounced in the case of the multilayer fully equilibrated at −2°C (Fig. 1 *C*) than in the case of the partially equilibrated multilayer for which the temperature was slewed from 7.5 to −2°C (Fig. 1 *B*). In the latter case the meridional (lamellar) diffraction pattern never fully acquires the characteristics of the pattern shown in Fig. 2 *C* even when the multilayer is maintained at −2°C for as long as 12–18 h after the temperature slewing (see below, Fig. 2). For these multilayers, if the temperature of partial dehydration of 7.5°C is restored, the initial diffraction pattern of Fig. 1 *A* is quickly restored, within 5 min. In the case of the multilayers partially dehydrated at low temperatures, i.e., fully equilibrated at 2–3 to −2°C, the diffraction pattern also reverts to a pattern typical of the higher temperatures upon reequilibration of the multilayer at 7.5–10°C, but this process requires a longer time, from 30 min to 2 h, depending on the individual multilayer. Except for this delay, the changes induced by temperature in the meridional diffraction pattern are completely reversible for all three experimental approaches utilized.

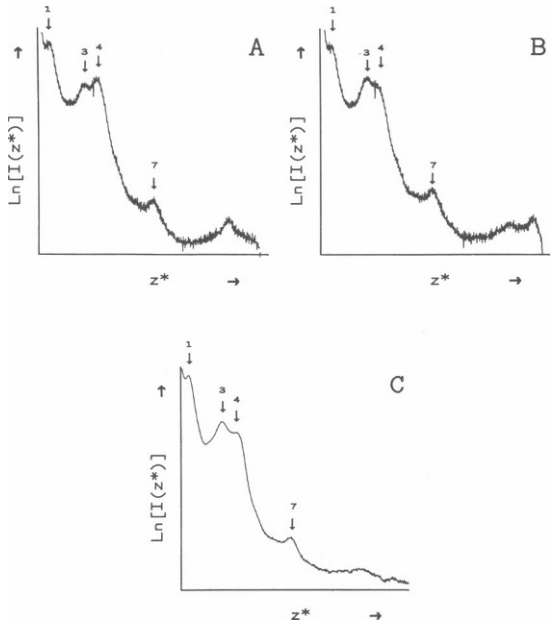

FIGURE 1 Typical meridional (lamellar) intensity functions $I(z^*)$ obtained from oriented SR membrane multilayers shown as the Ln x-ray counts vs. $z^* = (2\sin\theta/\lambda)$ position on a linear position-sensitive detector. (*A*) Diffraction from a multilayer fully equilibrated at 7.5°C. (*B*) Diffraction from the same multilayer after the temperature was slowly slewed to −2°C. (*C*) Diffraction from a multilayer fully equilibrated at −2°C. Numbers and arrows indicate expected positions of lamellar Bragg orders at $z^* = \ell/d$ for $d \sim 207$–211 Å and ℓ integer. The relative intensities of orders $\ell = 3$ and $\ell = 4$ undergo the most obvious change with the decrease of temperature, but the intensity of all other orders also varies. Diffraction patterns include the background scattering; the patterns in *A* and *B* represent a total collection time of 4 h, the pattern in *C* of 18 h.

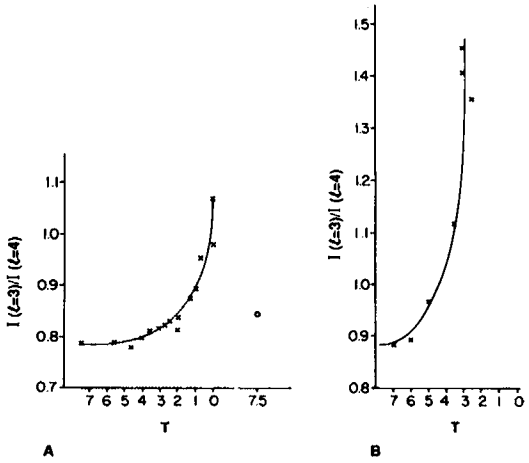

FIGURE 2 (*A*) For an oriented SR membrane multilayer fully equilibrated at 7.5°C the temperature was slowly (3 h and 40 min) slewed to 0°C. The meridional (lamellar) diffraction was collected at the intermediate temperatures and the peak intensities for orders $\ell = 3$ and $\ell = 4$ integrated:

$$\int_{\ell/d-\epsilon}^{\ell/d+\epsilon} I(z^*)\,dz^* = I(\ell).$$

The ratio of the two integrated intensities $I(\ell = 3)/I(\ell = 4)$ is plotted here vs. the temperatures. A structural transition occurs at ~2°C. Subjecting the sample to a temperature jump from 0 to 7.5°C quickly reverses the ratio $I(\ell = 3)/I(\ell = 4)$: the open circle corresponds to 5 min after this temperature jump. (*B*) A set of oriented SR membrane multilayers was partially dehydrated, with at least two multilayers at each of the temperatures indicated. The temperature dependence of the ratio $I(\ell = 3)/I(\ell = 4)$, calculated as in *A* for the multilayers fully equilibrated at each temperature, is shown by the curve. This ratio at ~2°C varies more rapidly than in *A*.

The change of the meridional diffraction pattern with temperature, expressed in terms of the changes in the relative integrated intensities of the diffraction orders

$$\int_{\ell/d-\epsilon}^{\ell/d+\epsilon} I(z^*)\, dz^* = I(\ell)$$

has been analyzed utilizing the experiments two and three described above. In Fig. 2 *A* the diagram shows, as a function of temperature, the behavior of the ratio of the integrated intensities of orders $\ell = 3$ and $\ell = 4$, which, of all orders, present the most obvious change. The curve is typical of experiments in which a single multilayer, partially dehydrated at 7.5°C, is slowly slewed over the range of temperatures from 7.5 to 0°C in ~4 h and thereby only partially equilibrated at each temperature indicated, immediately followed by a temperature reversal from 0 to 7.5°C occurring in 5 min. The diagram suggests that a major structural "transition" for this multilayer occurs at ~2°C and that it can be reversed by increasing the temperature. Fig. 2 *B* is a typical curve obtained for the sets of multilayers for which the multilayers were partially dehydrated and thereby fully equilibrated at each temperature between 7.5 and −2°C. It is similar to the curve in Fig. 2*A*, the only difference being that in this case the ratio $I(\ell = 3)/I(\ell = 4)$ varies more rapidly near the temperature of transition (~2°C). This is correlated with the more pronounced changes in the pattern observed for the multilayers fully equilibrated at the lower temperatures (Fig. 1).

Temperature Dependence of Equatorial Diffraction

Oriented multilayers of SR membranes for equatorial diffraction were prepared using the same procedure as for meridional (lamellar) diffraction. Fig. 3, *A–C*, are sectors of x-ray diffraction patterns recorded in 60 s by the two-dimensional detector; the background scattering, determined as described in Methods, has been removed from each pattern. For a multilayer fully equilibrated at 7.5°C (*A*) one radially broad ring is observed in the region dominated by diffraction from the lipid hydrocarbon chain packing in the membrane plane. For the same multilayer partially equilibrated at −2°C (*B*) a radially sharp ring at higher angle appears superimposed on the broad ring. In the case of the multilayer fully equilibrated at −2°C (*C*) the sharp ring at higher angle is somewhat more intense than the broad ring. As for the meridional (lamellar) diffraction, the phenomenon is totally reversible, that is the patterns in *B* and *C* can be reversed to the pattern in *A* by reequilibrating the multilayer at 7.5°C; for the multilayers partially dehydrated at the lower temperatures a delay is observed for this reversal, identical to the one occurring for the reversal of the meridional (lamellar) diffraction. The other main feature in these patterns consists of a radially

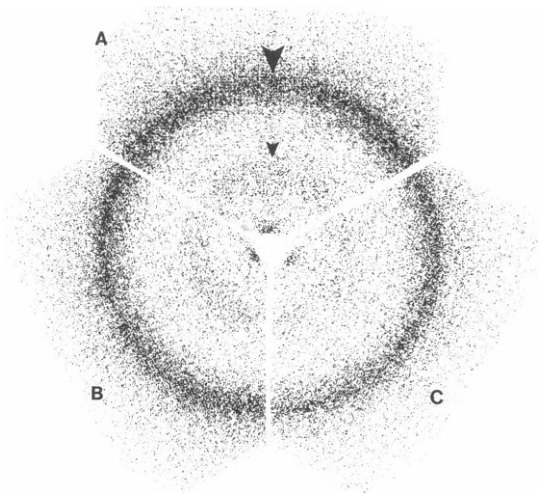

FIGURE 3 Equatorial diffraction patterns $I(r^*, \phi^*, z^* = 0)$ at normal incidence to the multilayer surface from an oriented SR multilayer fully equilibrated at 7.5°C (*A*), from the same multilayer partially equilibrated at −2°C (*B*), and from an oriented SR multilayer fully equilibrated at −2°C (*C*). In *A* only a radially broad diffraction ring, indicated by the larger arrow, occurs from the packing of the membrane lipid hydrocarbon chains in the membrane plane; in *B* and *C*, a radially sharp ring occurs at higher angle superimposed on the broad ring. The sharp ring disappears when the multilayers are reequilibrated at 7.5°C. The smaller arrow indicates the diffraction from protein α-helices.

broad ring at lower angle arising from the interference betwen α-helical polypeptide chains of the protein.

If the patterns of Fig. 3, *A* and *B*, are angularly integrated over $0 \le \phi^* \le 2\pi$ before background subtraction, the one-dimensional intensity functions $I(r^*, z^* = 0)$ of Fig. 4 are obtained. The function in the top of Fig. 4 represents the intensity function obtained from the integration of a two-dimensional equatorial pattern from a multilayer of DPL at room temperature, recorded under identical experimental conditions as for the SR equatorial patterns. It contains a radially sharp reflection, which is expected to occur at a Bragg spacing of ~1/4.2 $Å^{-1}$ at room temperature, characteristic of only frozen chains packed in crystalline domains over the membrane plane (19, 20). This reflection has been used to calibrate the r^* axis in Fig. 4. For the SR membrane multilayer fully equilibrated at 7.5°C, center of Fig. 4, the intensity function exhibits a broad symmetric peak at $r^* \sim 1/4.5$ $Å^{-1}$ characteristic of only melted chains with liquidlike (or disordered) packing over the membrane plane (19, 20). For the same multilayer partially equilibrated at −2°C, bottom of Fig. 4, the broad symmetric peak becomes asymmetric due to a sharp, more intense component on the higher-angle side of the peak at $r^* \sim 1/4.3$ $Å^{-1}$. This result is characteristic of "lipid lateral phase" separation where crystalline domains of frozen chains coexist within a liquidlike (or disordered) packing of melted chains over the membrane plane (21). These results are in agreement with the previous work of others (22).

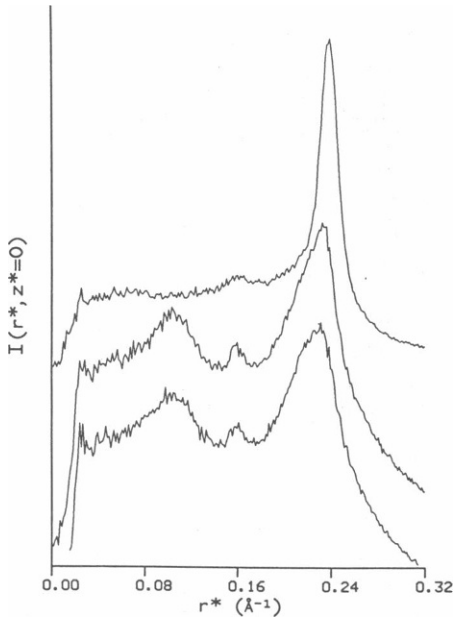

FIGURE 4 One-dimensional intensity functions $I(r^*, z^* = 0)$ obtained by angular ϕ^* integration of equatorial diffraction patterns as in Fig. 3, *A* and *B*. In the top of the figure, the intensity function for a DPL multilayer at room temperature; in the center, the intensity function for the multilayer fully equilibrated at 7.5°C; and in the bottom, the intensity function for the same multilayer partially equilibrated at −2°C. For details see the text.

The peaks at lower angle in the intensity functions of Fig. 4 are produced by background scattering (minor peak) and by the protein α-helical diffraction from the SR multilayers at $r^* \sim 1/10$ Å^{-1}.

Calculation of Membrane Electron Density Profiles

The meridional intensity functions $I(z^*)$ of Fig. 1, *A–C*, fully corrected, were subjected to two independent phasing methods for the calculation of the multilayer unit cell electron density profiles $\rho_{uc}(z)$, primarily the Generalized Fourier Synthesis Deconvolution Method (GFSDM [23]) which takes into account the disorder present in the multilayer lattice and assumes centrosymmetry of the unit cell membrane pair profile and also the iterative box refinement analysis (24). Both methods have been used successfully for membrane systems, including appropriate oriented membrane multilayers (5, 25). The GFSDM utilizes a model multilayer lattice interference function containing the lattice disorder parameters which is used to obtain a calculated meridional intensity function and a calculated multilayer profile autocorrelation function for each phase combination. These functions are compared with iteration of the lattice disorder parameters quantitatively with their corresponding experimental functions. The phase combination for which the calculated and experimental functions have the best fit is selected as the most probable. The results thereby provided by the GFSDM are shown in Fig. 5 for the multilayer fully equilibrated at 7.5°C, in Fig. 6 for the same multilayer partially equilibrated at −2°C, and in Fig. 7 for the multilayer fully equilibrated at −2°C (all profiles have been scaled to have the same ρ_{uc}^2 over the interval d). In the top of the figures, the experimental autocorrelation functions for the multilayer profiles, $Q_{exp}(z)$, the autocorrelation functions for the multilayer profiles calculated by GFSDM, $Q_{cal}(z)$, and the autocorrelation functions for the unit cell profiles, $Q_0(z)$ are shown; in the bottom of the figures the centrosymmetric unit cell electron density profiles $\rho_{uc}(z)$ for the membrane pair, representative of the two apposed membranes of a collapsed vesicle, are shown. The phases for the four lamellar diffraction maxima in the meridional data utilized to provide the profiles of Figs. 5

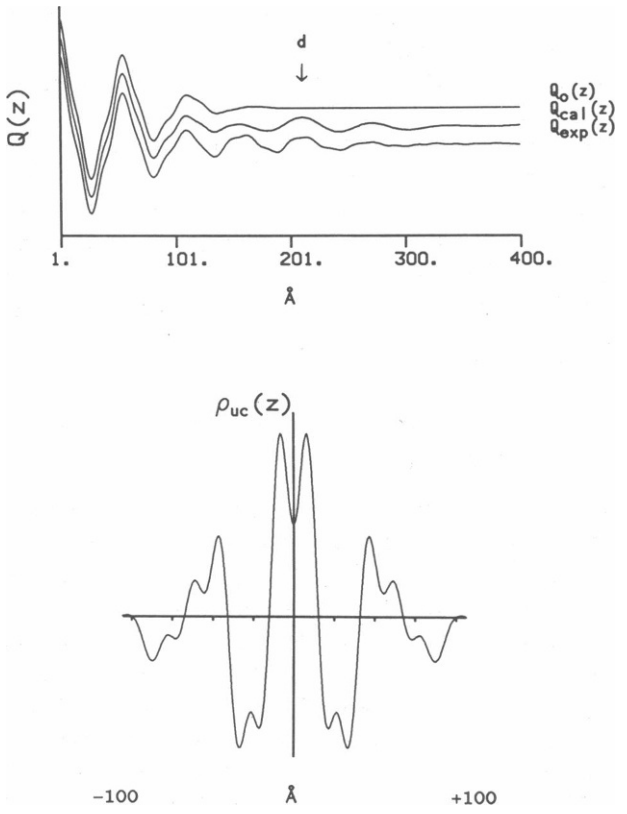

FIGURE 5 Results provided by the GFSDM analysis for the most probable phase combination for the meridional (lamellar) diffraction data at ~16 Å resolution of Fig. 1 *A*, SR membrane multilayer fully equilibrated at 7.5°C. In the top the Patterson functions $Q(z)$, vs. the real space coordinate z, calculated to $z = \sim 2d$: $Q_{exp}(z)$ is the autocorrelation function for the multilayer profile calculated directly from the corrected experimental intensity; $Q_{cal}(z)$ is the multilayer profile autocorrelation function obtained from GFSDM; $Q_0(z)$ is the autocorrelation function of the average unit cell profile; d at $z = 211$ Å is the lattice periodicity. In the bottom, $\rho_{uc}(z)$ is the average unit cell electron density profile on a relative scale vs. the real space coordinate z in Å, one divison 25 Å. The centrosymmetric unit cell profile extending from $-d/2$ to $+d/2$ contains the membrane pair, with a single membrane profile within $0 \leq |z| \leq 105.5$ Å.

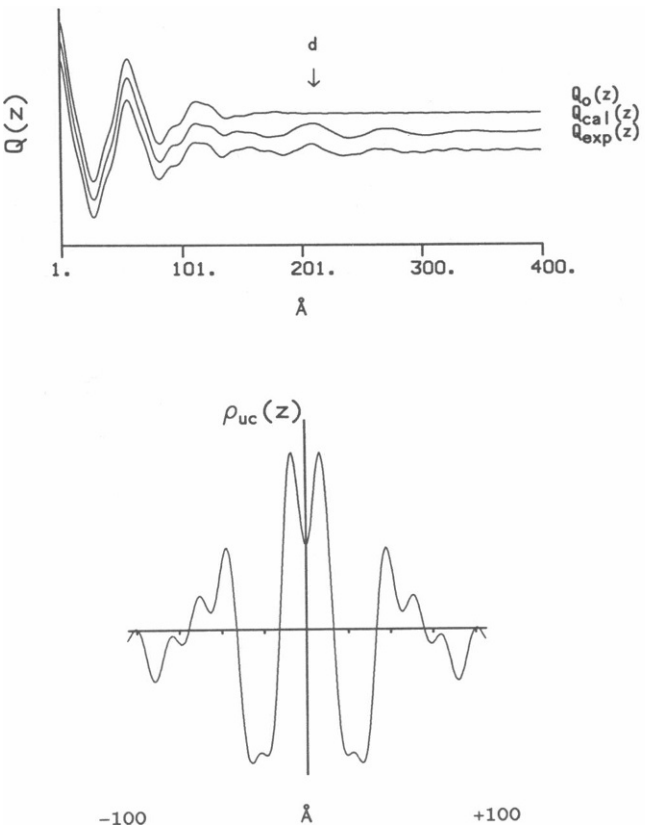

FIGURE 6 Functions calculated by GFSDM for the best phase combination for the meridional (lamellar) diffraction data of Fig. 1 *B* at a resolution of ~16 Å, same multilayer as in Fig. 5, subjected to a slewing of the temperature from 7.5 to −2°C and maintained at −2°C. The phase combination, *d*, and the extension of a single membrane profile are the same as for data in Fig. 5.

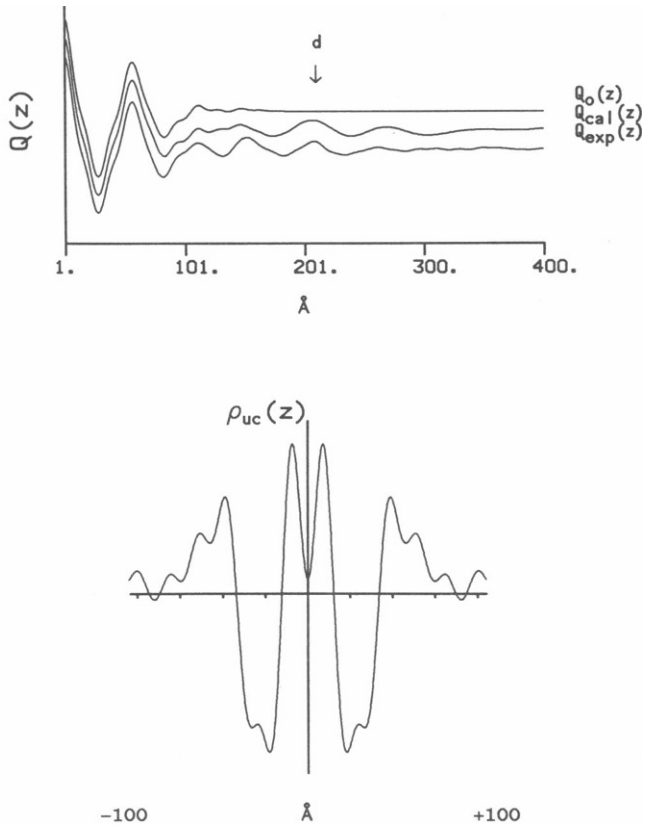

FIGURE 7 Functions calculated by GFSDM for the best phase combination for the meridional (lamellar) diffraction data of Fig. 1 *C* at ~17 Å resolution, the multilayer fully equilibrated at −2°C. The phase of the first diffraction order ($\ell = 1$) has the opposite sign with respect to the first order for the data in Figs. 5 and 6; $d = 207$ Å; the profile for a single membrane is contained within $0 \leq |z| \leq 103.5$ Å.

and 6 are the same (+ + − −), whereas for the data in Fig. 7 there is a reversal of the phase for the first order maximum (− + − −). This result, that the first order of the lamellar diffraction has opposite phase sign depending upon the temperature of partial dehydration, was tested further by applying independently the box refinement method to the experimental meridional intensity functions truncated at ~35 Å resolution, that is, inclusive of the first two regions of constant phase.[1] The truncation was applied based on consideration that the phases of these two regions, which dominate the meridional intensity function, cannot be affected by the phases of the weak orders at higher angle, in agreement with the Fourier sampling theorem. The solutions provided by box refinement are the electron density profiles for the membrane pair shown in Figs. 8 *A* (fully equilibrated at 7.5°C) and 9 *A* (fully equilibrated at −2°C). Figs. 8 *B* and 9 *B* show the centrosymmetric electron density profiles obtained by the GFSDM at the same resolution derived by truncation of the respective meridional diffraction data. Note that at this lower resolution the unit cell electron density profiles containing the membrane pair of Figs. 8 *B* and 9 *B* have one unresolved peak at the origin ($z = 0$) instead of two peaks at $z = \pm 8$ Å as in Figs. 5–7. It is readily apparent that the solutions provided by box refinement agree very well with the profiles chosen by GFSDM at the same resolution, confirming the phases of the first two regions of constant phase for the electron density profiles in Figs. 5 and 7. The lack of complete centrosymmetry of the profiles calculated by the box refinement is due to the large degree of freedom afforded by noncentrosymmetric phases utilized by the method. Applied in the case of the multilayer partially equilibrated at −2°C, the box refinement method also

[1]Because the correlation between membrane pairs (unit cells) in these multilayer lattices is rather weak, as indicated by the significant amount of lattice disorder present shown by the rapid decay to zero of $Q_{exp}(z)$ for $z \geq 2d$ (Figs. 5–7), the resulting weakly sampled meridional intensity function therefore very nearly represents the continuous Fourier transform modulus for a single membrane pair profile. Under these conditions of substantial lattice disorder an arbitrary trial function can be used in the iterative box refinement method to find a solution for the membrane pair electron density profile with the only requirement of constrained thickness for the membrane pair. This value was directly obtained from Figs. 5 and 7 from the value of z at which $Q_0(z)$ becomes zero ($Q_0[z]$ must be zero outside $\pm d$, the extension of the unit cell electron density profile, containing the membrane pair); a square pulse function of 105 Å width placed asymmetrically about the z origin was used as the trial function.

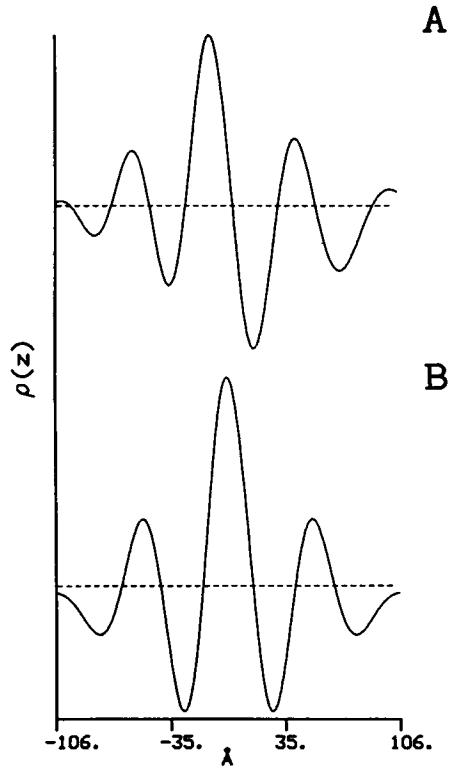

FIGURE 8 (*A*) Electron density profile for the membrane pair calculated by the box refinement method for the experimental intensity function for the multilayer fully equilibrated at 7.5°C truncated at ~35 Å resolution. The profile was obtained in 10 iterations, utilizing a square pulse function nonzero within $-55 \leq z \leq 50$ Å as the trial structure and a box size of 200 Å. The two apposed single membrane profiles are contained within $-105 \leq z \leq -11$ Å and $-11 \leq z \leq 105$ Å, z is the real space coordinate. (*B*) Low resolution profile at ~35 Å calculated for the same truncated intensity function utilizing the phase combination selected by GFSDM. One single membrane is contained within $0 \leq |z| \leq 105.5$ Å.

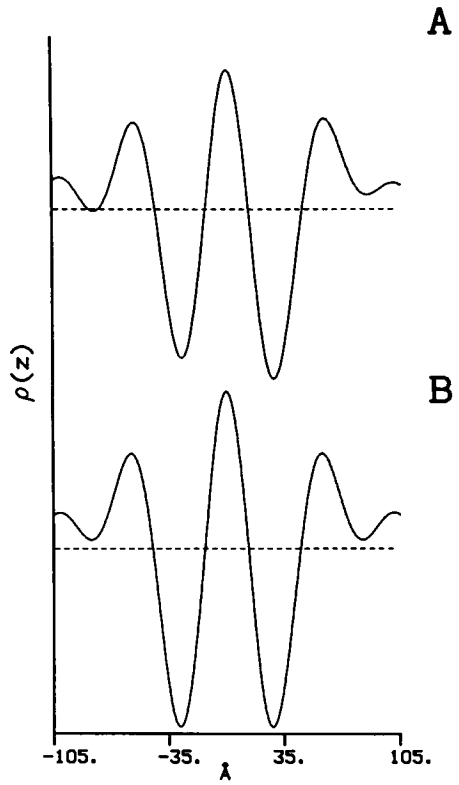

FIGURE 9 (*A*) Electron density profile for the membrane pair provided by box refinement for the experimental intensity function for the multilayer fully equilibrated at −2°C, truncated at ~35 Å resolution. The trial structure used was the same as in Fig. 8, the size of the box 203 Å, the number of iterations 10. The two apposed single membrane profiles are contained within $-105 \leq z \leq -3$ Å and $-3 \leq z \leq 105$ Å. (*B*) Low resolution profile at ~35 Å obtained for the same truncated intensity function utilizing the phases selected by GFSDM. One single membrane is contained within $0 \leq |z| \leq 103.5$ Å.

provides a solution in agreement with the GFSDM analysis (not shown).

DISCUSSION

The results described in Fig. 2, *A* and *B*, establish the occurence of a structural transition for the SR membrane multilayer profile at ~2°C. This temperature is clearly the critical temperature for the transition since it is confirmed either by subjecting single multilayers to a slow slewing of temperature around the transition temperature, or by fully equilibrating different multilayers at several temperatures around the transition temperature. The different slope of the curves near the temperature of transition in the two cases is correlated with the more pronounced changes in the meridional diffraction, with respect to the maridional diffraction from a multilayer fully equilibrated at 7.5°C, which are observed in the second case (Fig. 2 *B* vs. 2 *A*). This most likely indicates that the multilayers for which the temperature is slewed from 7.5 to −2°C do not reach full equilibrium at the intermediate temperatures within the time scale of the experiment (5 min/mean temperature value), or even within 12–18 h after the final temperature value. This is consistent with the fact that the electron density profiles for the SR membrane partially equilibrated and fully equilibrated at −2°C are not identical, having at least different phases for the first order reflections and different ratios for the third/fourth order reflections (see $\rho_{uc}(z)$ in Figs. 6 and 7). The profile in Fig. 6, partially equilibrated at −2°C, thus appears to be in an intermediate state between the profiles for the SR membrane in full equilibrium at 7.5°C (Fig. 5) and in full equilibrium at −2°C (Fig. 7).

The differences between the electron density profiles for the SR membrane at the lower and at the higher temperatures are statistically significant, because the changes in the meridional intensity functions are much larger than the counting statistics, as evidenced in the patterns in Fig. 1, and their phasing has been firmly established. To facilitate the interpretation of the profiles and their differences, they have been fitted with step-function models. In each case the step-function model for the two apposed membranes contain 16 steps of identical width and a step of smaller

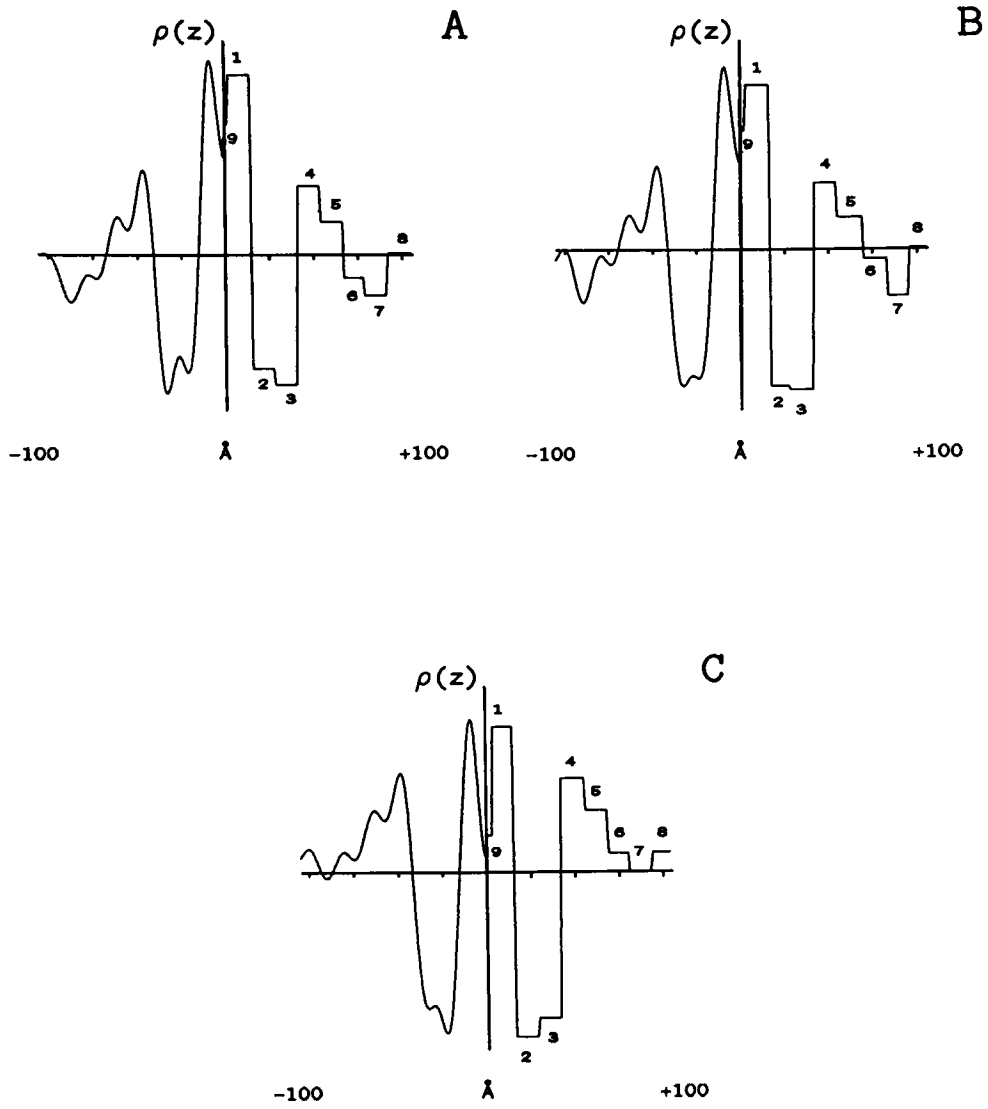

FIGURE 10 Step-function models for the profiles at 16–17 Å resolution of Figs. 5–7: on the left side are reproduced the electron density profiles for a single membrane from Figs. 5–7 extending from $z = -d/2$ to $z = 0$; on the right side the calculated step-function models for the apposed single membranes, extending from $z = 0$ to $z = +d/2$. The numbers identify the steps with the different regions of a single membrane profile as described in the text. In *A* the step-function model for the profile calculated for the multilayer fully equilibrated at 7.5°C, in *B* for the same multilayer partially equilibrated at −2°C, in *C* for the multilayer fully equilibrated at −2°C. The abscissa is the real space coordinate z in Å, one division, 25 Å.

width at the origin produced by the overlapping of two adjacent steps, the width of all steps thus being larger than the resolution limit $(2z^*_{max})^{-1}$. The magnitudes of the average electron density levels of the steps within the model profiles were refined to the experimental unit cell profile until the normalized least-square fit of the experimental and model unit cell structure factor obtained by Fourier transformation of the two functions was better than half a percent. The step-function models thus obtained are shown in Fig. 10, *A–C*, for the profiles of Figs. 5, 6, and 7, respectively. To compare the continuous electron density profiles with the correspondent step-function models, the Fig. 10 shows from $z = -d/2$ to $z = 0$ the continuous functions from Figs. 5–7 and from $z = 0$ to $z = +d/2$ the step-function models, only nine steps instead of 16. Relative to a single membrane profile, as previously interpreted from x-ray and neutron diffraction experiments, coupled with the deuteration of selected membrane molecular components (7), two steps (1 and 4) are fitted to the inner and outer lipid polar headgroup regions, two steps (2 and 3) to the lipid fatty acyl chain region of the inner and of the outer monolayer, four steps (5–8) are fitted to the extravesicular surface of the membrane (outside the lipid bilayer) extending to the edge of the unit cell; 9 labels the step at the origin of the unit cell corresponding to the intravesicular water space.

The differences between these step-function models in the case of a single multilayer fully equilibrated at 7.5°C (Fig. 10 *A*) and partially equilibrated at −2°C (Fig. 10 *B*) include a decrease of density for step 1 and 9, a small increase of density for steps 5 and 6, a major redistribution of density for steps 2 and 3 with density loss in 2 which brings the level of density of step 2 to nearly the same level of density of step 3. These differences appear much larger, but of the same character, when comparing the step-function models for the mutlilayer fully equilibrated at 7.5°C and the multilayer fully equilibrated at −2°C, Fig. 10 *A* vs. 10 *C*, in particular the level of density of step 2 decreases further to a level significantly lower than that of step 3. There is also a change with regard to the separation

of steps 1 and 4, 39 Å in Fig. 10 *A* and 40.5 Å in Fig. 10 *C*.

Given our previous interpretation of the SR membrane profile (7), these step-function models to the electron density profiles at this moderate resolution indicate the contribution of each membrane component to the changes occurring in the electron density profiles across the temperature-dependent structural transition. Relative to a single membrane profile three major changes take place with decreasing temperature across the transition: (*a*) an increase of the lipid polar headgroup separation across the SR lipid bilayer profile which reaches a maximum value of 1.5 Å in the case of the multilayer fully equilibrated at low temperature; (*b*) a change of the relative electron density in the lipid acyl chain region of the bilayer, with a significant loss of density in the chain region of the inner monolayer; (*c*) an increase of density over all the outer surface outside the lipid bilayer of the membrane extending to the edge of the unit cell. The changes described in *b* and *c* can be best accounted for in terms of a redistribution of the protein from the inner monolayer into the outer monolayer and into the outer surface of the membrane; because the protein present in this SR membrane preparation is nearly totally Ca^{2+}ATPase (26), this redistribution involves Ca^{2+}ATPase polypeptide. Conversely, a lipid redistribution between monolayers would seem to be excluded. It would require changes of the relative electron density in the polar headgroup region and hydrocarbon chains region of the outer monolayer matching the changes in the inner monolayer. Instead, corresponding to the loss of density in the inner monolayer an increase of density occurs largely on the outer surface of the membrane, a region that hosts the headpiece structure of the Ca^{2+}ATPase. Lipid redistribution is also a phenomenon too slow to occur in these experiments (7): the time scale of the slewing of temperature for the multilayer at 7.5 to -2°C is only on the order of 3–4 and its reversal takes only 5 min.

Concomitantly with redistribution of protein mass in the SR membrane profile, the temperature-dependent structural transition involves the formation of crystalline domains of frozen lipid chains in the SR membrane plane, i.e., "lateral lipid phase separation." Because the lipids in these domains have predominately full extended all-*trans* chains, the presence of frozen lipid chain domains can account for the increased average lipid polar headgroup separation across the lipid bilayer profile observed at -2°C (27). From the diffraction experiments presented, we cannot determine if crystalline lipid chain domains form preferentially in one monolayer of the membrane lipid bilyer nor can we reliably determine the relative number of lipid molecules involved. It is also impossible to determine if this lateral lipid phase separation for a portion of the lipids in the membrane directly induces the redistribution of the Ca^{2+}ATPase protein toward the outer extravesicular surface of the membrane profile or if the two phenomena occur independently. If one or more classes of lipids in the SR membrane were exchanged for lipids of different fatty-acyl chain composition (without altering the lipid class composition of the membrane) such that this upper characteristic temperature of the lateral lipid phase separation were altered, x-ray diffraction experiments analogous to the ones presented in this paper could determine if the structural change in the Ca^{2+}ATPase protein follows the upper characteristic temperature of the phase separation, thereby establishing casuality or conversely. Such lipid exchange has been successfully performed previously in the SR membrane utilizing either specific or nonspecific lipid exchange proteins (7).

The redistribution of protein mass from the inner to the outer monolayer under low-temperature conditions is in the opposite direction to the redistribution of protein mass induced by phosphorylation of the enzyme under identical low-temperature conditions (16) or at 7–8°C (11). In both cases time-resolved x-ray diffraction studies have in fact indicated that upon phosphorylation, Ca^{2+}ATPase protein mass moves from the outer towards the inner monolayer. Because the formation of the E_1~P intermediate is greatly slowed under such low-temperature conditions, it now appears that the low-temperature–induced structural changes in the enzyme profile are capable of slowing the calcium transport process because this process requires structural changes in the protein profile in the opposite direction for protein phosphorylation.

CONCLUSION

The study presented demonstrates a strong correlation between a temperature-induced lipid lateral phase separation in the SR membrane plane and significant structural changes in the SR membrane profile, which can be best accounted for in terms of a specific redistribution of Ca^{2+}ATPase protein mass within the membrane profile. Because the lifetime of the first phosphorylated intermediate of the Ca^{2+}ATPase, E_1~P, is considerably extented to at least several seconds for temperatures below this structural transition (as compared with only a few hundred milliseconds or less for temperatures above the transition), the structural transition could therefore be directly responsible for the "transient trapping" of this intermediate E_1~P. We note that the phase diagram for this membrane multilayer system is undoubtedly complex, depending significantly in addition to the water activity in the multilayer; this issue is currently under investigation.

Time-resolved x-ray diffraction studies performed at "low" temperature below this structural transition can now rigorously provide the profile structure for the SR membrane for which the enzyme is clearly transiently trapped in the first phosphorylated intermediate state (16). Previously, analogous studies at 7–8°C above this transition provided the profile structure for the SR membrane for which the Ca^{2+}ATPase is only predominately in the first phosphorylated intermediate state (11).

This work was supported by a grant from the National Institutes of Health, NIH HL-18708, to J. K. Blasie.

Received for publication 25 August 1987 and in final form 13 May 1988.

REFERENCES

1. Ebashi, S., M. Endo, and I. Ohtsuki. 1969. Control of muscle contraction. *Rev. Biophys.* 2:351–384.
2. Weber, A., R. Herz, and J. Reiss. 1963. On the mechanism of the relaxing effect of fragmented sarcoplasmic reticulum. *J. Gen. Physiol.* 46:679–702.
3. Duggan, P. F., and A. Martonosi. 1970. Sarcoplasmic reticulum. IX. Permeability of sarcoplasmic reticulum membranes. *J. Gen. Physiol.* 56:147–167.
4. DeMeis, L., and A. L. Vianna. 1979. Energy interconversion by the Ca^{2+}-dependent ATPase of the sarcoplasmic reticulum. *Annu. Rev. Biochem.* 48:275–292.
5. Herbette, L. G., J. Marquardt, A. Scarpa, and J. K. Blasie. 1977. A direct analysis of lamellar x-ray diffraction from hydrated oriented multilayers of fully functional sarcoplasmic reticulum. *Biophys. J.* 20:245–272.
6. Herbette, L. G., A. Scarpa, J. K. Blasie, C. T. Wang, A. Saito, and S. Fleischer. 1981. A comparison of the profile structures of isolated and reconstituted sarcoplasmic reticulum membranes. *Biophys. J.* 36:47–72.
7. Herbette, L. G., P. DeFoor, S. Fleischer, D. Pascolini, A. Scarpa, and J. K. Blasie. 1985. The separate profile structures of the calcium pump protein and the phospholipid bilayer within isolated sarcoplasmic reticulum membranes determined by x-ray and neutron diffraction. *Biochim. Biophys. Acta.* 817:103–122.
8. Pierce, D., A. Scarpa, D. R. Trentham, M. R. Topp, and J. K. Blasie. 1983. Comparison of the kinetics of calcium transport in vesicular dispersions and oriented multilayers of sarcoplasmic reticulum membranes. *Biophys. J.* 44:365–373.
9. McCray, J. A., L. G. Herbette, T. Kihara, and D. R. Trentham. 1980. A new approach to time-resolved studies of ATP-requiring biological systems: laser flash photolysis of caged ATP. *Proc. Natl. Acad. Sci. USA.* 77:7237–7241.
10. Pierce, D., A. Scarpa, M. R. Topp, and J. K. Blasie. 1983. Kinetics of calcium uptake by the sarcoplasmic reticulum vesicles using flash photolysis of caged adenosine 5'-triphosphate. *Biochemistry.* 22:5254–5261.
11. Blasie, J. K., L. G. Herbette, D. Pascolini, V. Skita, D. H. Pierce, and A. Scarpa. 1985. Time-resolved x-ray diffraction studies of the sarcoplasmic reticulum membrane during active transport. *Biophys. J.* 48:9–18.
12. Pascolini, D., L. G. Herbette, V. Skita, F. Itshak, A. Scarpa, J. K. Blasie. 1985. "Trapping" a structurally distinc intermediate in the Ca^{2+} uptake reaction of the sarcoplasmic reticulum by time-resolved x-ray diffraction. *Biophys. J.* 47:454a. (Abstr.)
13. Pascolini, D., L. G. Herbette, V. Skita, F. Itshak, A. Scarpa, and J. K. Blasie. 1986. A structural origin for the low-temperature trapping of E~P in isolated sarcoplasmic reticulum. *Biophys. J.* 49:567a. (Abstr.)
14. Blasie, J. K., D. Pascolini, L. Herbette, D. Pierce, F. Itshak, V. Skita, and A. Scarpa. 1986. Time-resolved structural studies of the sarcoplasmic reticulum membrane. *Biophys. J.* 49:110–111.
15. Pascolini, D., L. Herbette, V. Skita, A. Scarpa, and J. K. Blasie. 1987. Changes in the sarcoplasmic reticulum membrane profile upon E~P formation at ~15 Å resolution. *Biophys. J.* 51:346a. (Abstr.)
16. Pascolini, D., L. G. Herbette, V. Skita, F. Asturias, A. Scarpa, and J. K. Blasie. 1988. Changes in the sarcoplasmic reticulum membrane profile induced by enzyme phosphorylation to E_1~P at 16 Å resolution via time-resolved x-ray diffraction. *Biophys. J.* 54:679–688.
17. Pascolini, D., F. Asturias, and J. K. Blasie. 1987. Moderate resolution profile structure of the sarcoplasmic reticulum mebrane under "low" temperature conditions. *Biophys. J.* 51:347a. (Abstr.)
18. Franks, A. 1955. An optically focusing x-ray diffraction camera. *Proc. Phys. Soc. Lond. Sect. B.* 68:1054–1064.
19. Luzzati, V. 1968. X-ray diffraction studies of lipid-water systems. *Biol. Membr.* 1:71–123.
20. Luzzatti, V., and A. Tardieu. 1974. Lipid phases: structure and structural transitions. *Annu. Rev. Phys. Chem.* 25:79–94.
21. McConnell, H. M., P. Devaux, and C. Scandella. 1972. Lateral diffusion and phase separation in biological membranes. *In* Membrane Research. C. F. Fox, editor. Academic Press, New York. 27–37.
22. Davis, D. G., G. Inesi, and T. Gulik-Krzywicki. 1976. Lipid molecular motion and enzyme activity in sarcoplasmic reticulum membrane. *Biochemistry.* 15:1271–1276.
23. Schwartz, S., J. E. Cain, E. Dratz, and J. K. Blasie. 1975. An analysis of lamellar x-ray diffraction from disordered membrane multilayers with application to data from retinal rod outer segments. *Biophys. J.* 15:1201–1233.
24. Stroud, R. M., and D. A. Agard. 1979. Structure determination of asymmetric membrane profiles using an iterative Fourier method. *Biophys. J.* 25:495–512.
25. Jayaraman, U., T. Chang, T. G. Frey, and J. K. Blasie. 1987. Electron density profile of two-dimensionally crystalline membranous cytochrome c oxidase at low resolution. *Biophys. J.* 51:475–486.
26. Meissner, G., G. E. Conner, and S. Fleischer. 1973. Isolation of sarcoplasmic reticulum by zonal centrifugation and purification of Ca^{2+} pump and Ca^{2+} binding proteins. *Biochim. Biophys. Acta.* 298:246–269.
27. Linden, C. D., J. K. Blasie, and C. F. Fox. 1977. A confirmation of the phase behavior of *Escherichia coli* cytoplasmic membrane lipids by x-ray diffraction. *Biochemistry.* 16:1621–1625.